ADVANCED SUSTAINABLE SYSTEMS
www.advsustainsys.com

Hybridization of Salt Hydrates with Solid–Solid Phase Change Materials: A Novel Pathway to Sorption Thermochemical Materials Manufacturing

Anabel Palacios, Maria Elena Navarro, Camila Barreneche, and Yulong Ding*

Major advancements are needed in the thermochemical energy storage (TCES) field to bring the technology to commercial levels. The current research strategies are focused on improving heat and mass transfer using different supporting materials to achieve mechanical integrity during storage. However, these strategies are still under development, and they have not overcome the lab scale yet. This work explores novel matrices to expand the material database for TCES composites. Pure structural matrices (cellulose) and novel matrices with storage potential (polymeric solid–solid phase change materials) are selected and combined with three well-known thermochemical materials (TCMs) ($MgSO_4 \cdot 6H_2O$, $SrBr_2 \cdot 6H_2O$ and $MgCl_2 \cdot 6H_2O$), providing evidence of hybridized composites with storage capacity up to 2.4 GJ m^{-3} with a 25–20 wt% of polymeric matrix. The polymer content is found to act as a nucleating agent in the magnesium sulfate crystallization process forming a synthetic monohydrate crystalline phase (Kieserite) and inhibiting the formation of the amorphous phase. The effect of the matrix is proved to induce certain structural deformation or changes not observed in the pure TCM sorption process. This phenomenon has the potential to benefit the stabilization of the TCM, e.g., inhibition of the formation of amorphous phase in magnesium sulfate composites.

1. Introduction

Thermal energy storage (TES) is a key enabling technology with an important role in future energy systems that will increase dispatchability, allow peak load shifting, and decarbonize the energy network. TES has been traditionally classified into three technology categories: sensible (STES), latent (LHTES), and thermochemical energy storage (TCES). STES has been in large-scale industrial applications for over 200 years (e.g., blast furnace iron-making), whereas LHTSE has just started to be implemented in industry. Meanwhile, TCES based has the potential to provide efficient, compact, and long-duration storage of thermal energy, but is still at a very low technology readiness level (TRL).

Major advancements are needed to meet performance and cost targets; fundamental challenges such as heat and mass transfer limitations, difficulties in temperature control during the charge/discharge processes, life span, and cost-effectiveness are impeding its development. To date, the thermochemical material (TCM) research community has mainly been focused on addressing these challenges by proposing new reactive materials with high energy densities[1] and improving heat and mass transfer using different supporting materials to achieve mechanical integrity during charging/discharging cycles. These new materials developed are being studied to establish a framework for evaluating their performance at the system level.[2] However, these strategies are still under development, and they have not overcome the lab scale yet. Moreover, still, there is a lack of large-scale manufacturing routes that prevents an assessment of the links between composite production, properties, and performance at the system level scale required.

Aiming to tackle these challenges, the authors have proposed the three-in-one concept in a paper published in 2019.[3] The three-in-one system combines the three traditional TES technologies: STES, LHTES, and TCES in a three-in-one system. Within the hybridized composite material, the LHTES is stored by the phase change material (PCM), the TCES is stored through the thermochemical material (TCM), and the sensible heat is stored by both PCM and TCM, as the heat is proportional to the temperature gradient applied. Following the previous work, in this study, the authors aim to explore the hybridization of thermochemical material with two different kinds of matrices: 1) structural matrix without storage potential and 2) structural matrix with storage potential.

The eventual goal of this research is to provide more evidence and insights into thermochemical material hybridization,

A. Palacios, M. E. Navarro, C. Barreneche, Y. Ding
School of Chemical Engineering
University of Birmingham
Birmingham B152TT, UK
E-mail: anabel.palacios@hslu.ch

The ORCID identification number(s) for the author(s) of this article can be found under https://doi.org/10.1002/adsu.202200184

DOI: 10.1002/adsu.202200184

emphasizing its novelty and potential to revolutionize the storage sector. In this paper, we select four thermochemical materials and four novel matrices with storage potential that are characterized and cycled at different tablet sizes: lab-scale (1 g) to scale-up (20 g). Different polymeric solid–solid PCM materials are proposed as a structural matrix with storage potential and cellulose is proposed as the solely structural matrix, while the TCM is proposed to be sorption-based. More details about paper's content and guidelines are included in the following section of the paper.

2. Novelty and Potential

Novel matrices and strategies for thermochemical material structural stabilization are required to unlock the current TRL level of thermochemical energy storage (ES) technology. Researchers have mainly provided solutions based on composite salt stabilization[4] that require complicated multistep manufacturing processes by sacrificing the inherent energy density of TCMs, given the high structural matrix load required needed. Conventional ceramic-based and graphite-based matrices have proven to increase the cyclability of TCM but at expense of the energy density reduction and by providing a rigid structure.[5,6] To explore the full potential of TCMs an elastic and accommodating matrix is needed to assist in the contraction/expansion during the charging/discharging processes. Besides, to retrieve the highest energy density from the system a matrix with storage potential can provide a surplus of energy stored aside from the main storage media (thermochemical-based). In this paper, we change the approach to tackling TCM structural challenges by exploring non-conventional matrices that have the potential to bring a new generation of hybridized composites with superior performance and tailored properties. The envisioned hybridized composite provides higher TCM loading, higher practical energy density, larger cyclability, and greater structural stability. Besides, the hybridized system pathway opens up new manufacturing routes such as extrusion and 3D printing given the use of polymer materials for TCM stabilization while making this technology more economically attractive for commercial development.

3. Scope and Guidance

This paper is targeted to scientists and engineers working in the ES field, specifically experimentalists who are interested in either of the TES technologies, thermochemical or latent heat storage.

This paper works as an extension of the concept presented in the previous work, where the three-in-one storage strategy was envisioned and explored.[3] In this work, the hybridized composite is formulated starting with the material screening to storage media conceptualization through the following steps experiment design, process methodology optimization, and manufacturing scale-up. The paper is organized in the following manner: In the first section, Section 4 of the paper, a brief literature review is provided to screen the components of the hybrid composite: thermochemical materials and novel matrices. Section 5 includes the specifications of the experimental research (e.g., materials, methods, and equipment) and the manufacturing process proposed. The envision of the hybridized composite is described in Section 6, the section is divided into two main parts; Part 1, the study of components compatibility at lab scale and Part 2, the study of selected working pairs for scaling up to 20 g tablet size. Besides, experimental validation is performed in Section 6, revealing interesting properties of the novel matrices. The results are discussed eventually aiming to understand how the three-in-one composite works and the potential that this material can bring. To wrap up a conclusion section is included with the main highlights and takeaways of the paper.

4. Literature Review

In this section, the thermochemical materials and novel matrices selected in this investigation are presented. From the literature, some of them are selected and proposed for the hybridized composite; four thermochemical materials, three solid–solid phase change materials (SS-PCM) (structural matrix with storage potential) and one pure structural matrix.

4.1. Thermochemical Materials

TCS materials store thermal energy through the heat effect of reversible chemical reactions and/or sorption/desorption processes. TCS fall broadly into two main groups chemical reaction (strictly thermochemical storage without sorption) and sorption energy storage.[7] In the sorption process, the heat is stored by breaking the binding force between the sorbent and the sorbate in terms of chemical potential.[8] Sorption is commonly a simultaneous chemical/adsorption process based on the reversible reaction of solids and gas, which are generally assumed to be hydrated with a high number of crystal water molecules (salt hydrates). For building applications, low-temperature thermochemical energy storage materials such as $MgSO_4{\cdot}7H_2O$, $SrBr_2{\cdot}6H_2O$, and $MgCl_2{\cdot}6H_2O$ have been intensively developed and optimized during the past few years.[9–17] The temperature range of interest in this work was set from 25 to 150 °C, which is suitable for building applications and waste heat recovery. Among the commercially available candidates, we selected four TCMs that broadly represent the most promising sorption materials (bromides, chlorides, and sulfates) as well as the ones most reported in the literature. The following reactions are studied

$$MgCl_2 \cdot 6H_2O \leftrightarrow MgCl_2 \cdot 2H_2O + 4H_2O \quad T; \sim 30\,^{\circ}C - 130\,^{\circ}C \tag{1}$$

$$SrBr_2 \cdot 6H_2O \leftrightarrow SrBr_2 \cdot 1H_2O + 5H_2O \quad T; \sim 60\,^{\circ}C - 90\,^{\circ}C \tag{2}$$

$$MgSO_4 \cdot 6H_2O \leftrightarrow MgSO_4 \cdot 1H_2O + 5H_2O \quad T; \sim 30\,^{\circ}C - 150\,^{\circ}C \tag{3}$$

4.2. Novel TCM Matrices

The novel matrices are divided into a pure structural matrix and a structural matrix with storage potential. In the following sections, the criteria for the matrix selection and their attributes are described.

Table 1. Key properties of screened SSPCMs and alternative matrix.

Kind of matrix	Matrix	Latent heat [J g^{-1}]	Phase change temperature [°C]	Crystallization temperature [°C]	Crystallization enthalpy [J kg^{-1}]	Thermal conductivity [W m^{-1} K^{-1}]	Specific heat capacity [J g^{-1} k^{-1}]	Volume expansion [%]	Degradation temperature [°C]	Autoignition point [°C]	Price [£ kg^{-1}]
Structural matrix with storage potential polymeric SS-PCM	MDI	108.7[23]	38[28] 56.7[23] 40[38]	70–90[39]	–	0.126[a]	1.067[23]	–	240[40]	211[38]	3–5[b]
	PEO	52.8[23]	66–75[41]	40.6–134.7[23]	−32 to (−40)[23]	0.2[42]	40–140[23]	–	360[43]	370[a]	5–10[b]
	HDPE	180–210[44] 178.6[45]	130.8[46] 130–135[45] 130–131[47]	110–120[45]	−189[45]	0.48[a] 0.44 0.3[44]	1.8[48]	–	250–300[49]	350[a]	1–5[b]
Pure structural matrix	Cellulose	–	–	–	–	0.04[a]	–	–	200–30[50]	255[a]	4–10[b]

[a] chemical database; [b] manufacturer price range.

4.2.1. Pure Structural Matrix: Cellulose

The authors consider a pure structural matrix, a matrix that does not influence the storage process (aside from structural interactions) and does not store energy in its single structure. There are currently in the literature available options for pure structural support of thermochemical materials. Among them, graphite, vermiculite and magnesium oxide are the ones that have shown greater potential for applicability in TCS.[4,18] Other less researched options such as pure structural matrices are attapulgite, activated carbon and cellulose.[18] Cellulose has been studied with the impregnation of PCM,[19,20] as well as a polymeric blend,[21,22] and as a backbone of polymeric matrixes, showing the best efficiencies among the options available.[23] Besides, cellulose has been studied by one author as a matrix of TCM materials,[24] concluding that the cellulose fibers present may improve the mechanical stability of the salt bed. Given that cellulose has not been yet widely studied, here we choose to explore the compatibility and cyclability of cellulose with a variety of TCM materials.

4.2.2. Structural Matrix with Storage Potential: Solid–Solid Phase Change Material

Structural materials with storage potential in use for thermochemical storage materials stabilization are known as "composite in porous salt matrices."[4] Among the options proposed in the literature, the main alternatives are a range of zeolites and silica gel.[18] In this paper, we follow a ground-breaking approach as part of the work presented by Palacios et al.,[3] and we target the use of structural matrices with storage potential to SS-PCM.

SS-PCMs of interest for the hybridized composite are polyalcohols and polymeric, as inorganic and organometallic do not meet the screening prerequisites and can lead to chemical incompatibilities due to their chemical nature.[25] Many linear polymers undergo reversible solid-solid phase transitions upon cooling from their molten amorphous state. Unlike other PCMs, polymeric materials are not susceptible to phase segregation, although they are sensitive to degradation upon thermal and thermo-oxidative cycles.[26] This selection agrees with the scientific community who stated that polyalcohols and polyethylenes are the most promising solid–solid PCMs.[27] Among all the polymeric SS-PCMs three were selected for the three-in-one selection study MDI, PEO, and HDPE.

MDI has a melting point of around 38 °C. It forms insoluble dimers when stored above the melting point and it tends to crystallize.[28] MDI has been used as the hard segment in high-performance SSPCMs copolymers combined with PEG/PE[29–31] and PEG/polyurethane phase change materials.[32] PEO has been widely used in the fields of solar energy utilization, waste heat recovery, electric energy storage, drug-controlled release, and tissue engineering. This material has the added value of allowing for chemically modified PEOs and polymer/PEO blends exhibit unique solid–solid phase transition behavior and are efficient thermal energy storage materials.[22,23,31,33] HDPE has been used as a polymeric matrix for shape stabilized phase change materials.[59,60] HDPE itself can also be used as a polymeric phase change material.[34–37] HDPE has a melting point (solid–viscous transition) of ≈135 °C, a high specific heat of ≈2 kJ kg^{-1} K^{-1}, and a decent latent heat of fusion of ≈164 kJ kg^{-1}.[64] Among all the semicrystalline polymeric materials that can be used as a PCM,[26] HDPE is the one that shows the highest latent heat of fusion at temperatures lower than 150 °C (**Table 1**).

4.3. Working Pairs

In **Figure 1** the schematics of the potential storage matrices for the hybridized system are represented by the charging and discharging for the structural matrix with storage potential on the left and the solely structural matrix on the right. In the figure there are different processes taking place simultaneously during the charging and the discharging: (a) the salt hydrate (TCM) undergoes hydration while releasing heat through an endothermic reaction; (b) involves the dehydration of the salt hydrate (TCM) while absorbing heat through an exothermic reaction; (c) involves the solidification of the polymeric matrix to discharge the stored energy the SSPCM is cooled below its crystallization temperature and held below the crystallization temperature until charged again; (d) in this step, the PCM is heated above its melting temperature to charge and held at this temperature until the discharging step. Since the polymeric material is permeable to water no interaction between matrix and water is expected in

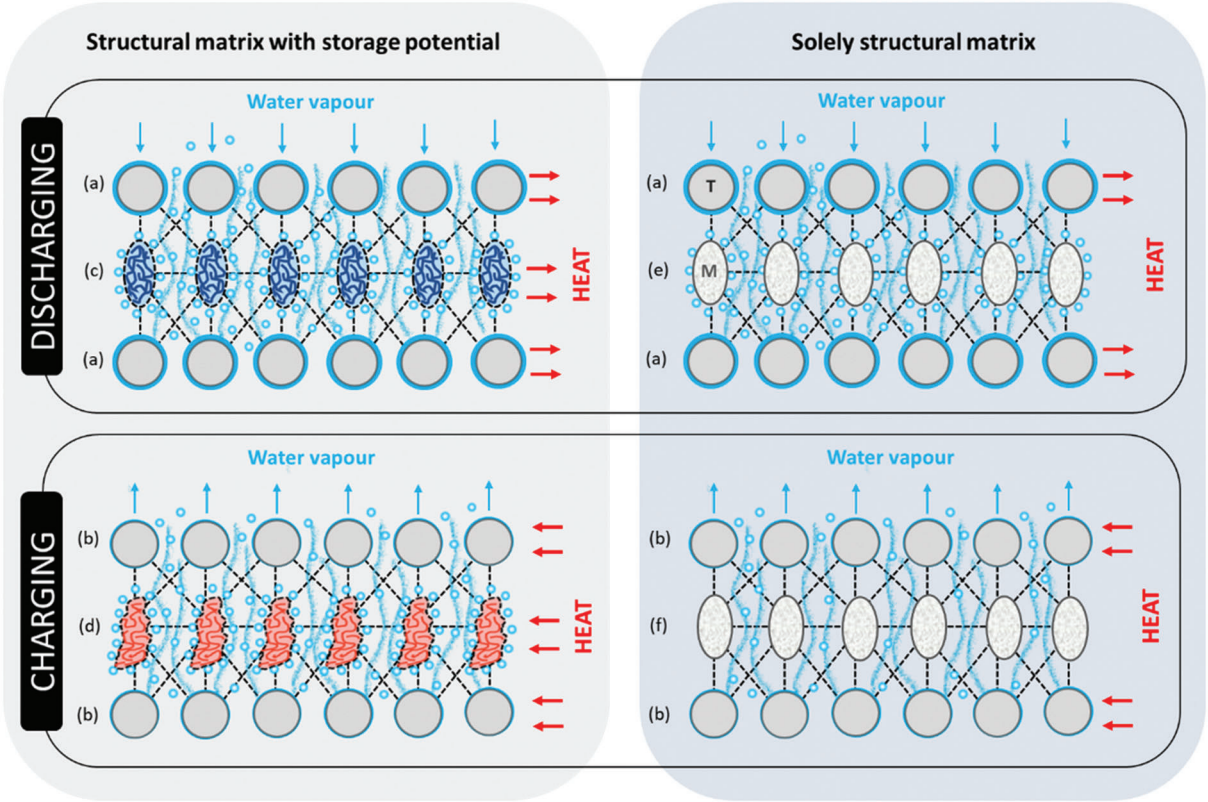

Figure 1. The schematics of the working mechanism during the charging and discharging process of hybridized composite with structural matrix and structural matrix with storage potential. (T) for thermochemical storage material and (M) for matrix material.

this case. Step (e) and (f) involves the structural support from the cellulose matrix during hydration and dehydration, which does interact with water given that its structure provides a good disposition for water absorption 4%–5% (w/w).[51] Varying the crystallinity of cellulose powder is expected to cause changes in the moisture content.

The use of polymeric materials as a structural matrix with storage potential bring great advantages that involve: (1) higher potential of energy storage; (2) higher loading of TCM; (3) flexible matrix to accommodate volume change; (3) permeable structure to water; and (4) easy and degree of freedom to shape. However, they can be susceptible to degradation upon thermal and thermo-oxidative loads. Thus, we need to ensure that we work within safe working conditions. Whereas the use of cellulose as a solely structural matrix ensures (1) higher TCM loading; (2) stable matrix for structural stability; (3) matrix inert to water (low percentages of water absorbance); and (4) easy to pelletize. However, cellulose does not provide a flexible structure which might lead to the cracking of the composite because of the contraction/expansion of the thermochemical material.

Overall, both matrices exhibit challenges and advantages that should be studied under operational conditions. The criteria for the working pairs formulation were to combine a TCM with one novel matrix for TCM stabilization, among them; three SS-PCMs (MDI, HDPE, PEO) and one pure structural matrix (cellulose). The potential for working pairs combinations is limited by the possible temperature-wise combination, see **Table 2**.

5. Experimental Section

5.1. Materials

The TCMs selected for this study are magnesium sulfate heptahydrate ($MgSO_4{\cdot}7H_2O$), magnesium chloride (anhydrous $MgCl_2$), and strontium bromide ($SrBr_2{\cdot}6H_2O$). Magnesium sulfate analytical reagent grade (CAS: 10034-99-8, MW: 246.48) was supplied by Fisher Scientific, strontium bromide from Sigma Aldrich, and magnesium chloride was purchased in anhydrous form from Acros Organics (CAS: 7786-30-3, MW: 95.21, Pure). The PCMs selected were high-density polyethylene (HDPE; CAS: 9002-88-4, MFI: 3.2) supplied by Matrix company, 4,40-diphenylmethane diisocyanate (MDI) supplied by Acros Organics ($C_{15}H_{10}N_2O_2$) in flakes, 98% (CAS: 101-68-8, MW: 250.26), and polyethylene oxide ($-CH_2CH_2O-$)*n*, from Alfa Aesar (CAS: 25322-68-3, MW: >5 000 000). The cellulose matrix was the microcrystalline cellulose powder from MPBio (CAS: 9004-34-6, MW: N/A).

5.2. Characterization Techniques

Different ratios of TCM and matrix (SS-PCM and cellulose), both in powder form, were mixed and ground into a homogeneous mixture. Two kinds of tablets were prepared: 1 g for the lab-scale study and 20 g for the scale-up study. For the lab-scale, 0.95 g ± 0.05 g of TCM/PCM mixtures were pressed into tablets shape of 13 mm diameter and 10 mm thickness using the Lloyd LS100

Table 2. Potential working pairs combining TCMs with SSPCM and alternative matrix..

	Pure structural matrix	Structural matrix with storage potential		
TCM	Cellulose	MDI (T_m: 40 −50 °C)	PEO (T_m: 66 −75 °C)	HDPE (T_m: 130 −135 °C)
$MgCl_2$•$6H_2O$ (T_R: 30 −130 °C)		X	X	X
$SrBr_2$•$6H_2O$ (T_R: 60 −90 °C)	X	X	X	
$MgSO_4$•$6H_2O$ (T_R: 25 −150 °C)	X	X		X

T_R refers to the temperature range for the thermochemical reaction; T_m refers to the phase change temperature.

Table 3. Summary of characterization conditions of the novel TCS composites.

Equipment	$MgSO_4$-PCM	$MgCl_2$-PCM	$SrBr_2$-PCM
STA	Heating: 30–150 °C at 1°C min^{-1} Isotherm: 1 h at 150 °C Cooling: 150 to 30 °C at 2.5 °C min^{-1} Hydration: 30 °C 80% R.H. for 2.5 h	Heating: 30–130 at 1 °C min^{-1} Isotherm: 1 h at 130 °C Cooling: 130 to 30 °C at 2.5 °C min^{-1} Hydration: 30 °C 40% R.H. for 2 h	Heating: 30–90 °C at 1 °C min^{-1} Isotherm: 1 h at 90 °C Cooling: 90 to 30 °C at 2.5 °C min^{-1} Hydration: 30 °C 50% R.H. for 2 h
Humidity chamber	Heating: 30–150 °C at 1 °C min^{-1} Isotherm: 1 h at 150 °C Cooling: 150 to 30 °C at 2.5 °C min^{-1} Hydration: 30 °C 80% R.H. for 2.5 h	Heating: 30–130 at 1 °C min^{-1} Isotherm: 1 h at 130 °C Cooling: 130 to 30 °C at 2.5 °C min^{-1} Hydration: 30 °C 40% R.H. for 2 h	Heating: 30–90 °C at 1 °C min^{-1} Isotherm: 1 h at 90 °C Cooling: 90 to 30 °C at 2.5 °C min^{-1} Hydration: 30 °C 50% R.H. for 2 h
XRD high temperature	Heating: 25–150 °C at 1 °C min^{-1} Temperature steps: 25, 30, 40, 70, 90, 120, 150 °C Isotherm: 150 °C at 30 min Cooling: 150 to 25 °C Temperature steps: 150 and 25 °C Air flow 100 mL min^{-1}	Heating: 25–140 °C at 1 °C min^{-1} Temperature steps: 25, 30, 40, 70, 90, 120, 140 °C Isotherm: 140 °C at 30 min Cooling: 140 to 25 °C Temperature steps: 140 and 25 °C Airflow 100 mL min^{-1}	Heating: 25–150 °C at 1 °C min^{-1} Temperature steps: 25, 30, 40, 70, 90, 120, 150 °C Isotherm: 150 °C at 30 min Cooling: 150 to 25 °C Temperature steps: 150 and 25 °C Airflow 100 mL min^{-1}
Pressing machine	Lab-scale study: 0.95 g ± 0.05 tablet 90 MPa 1.2 min Dimensions: 13 mm diameter and 10 mm thickness Scale-up study: 19.5 ± 0.5 g tablets 40 MPa 1.5 min. Dimensions: 30 mm diameter and 25 mm thickness		

Plus Materials Testing Machine supplied by Lloyd Instruments Company (UK). The operating pressure and holding time were set to 90 MPa and 1.2 min, respectively. 19.5 g ± 0.05 g with 30 mm diameter and ≈25 mm thickness tablets were pressed using an operating pressure and holding time of 40 MPa and 1.5 min, respectively. Three pellets for each formulation and cycling test were prepared. The compacted composites were tested to determine the cycling stability after charging/discharging cycles. The energy stored (STA), chemical stability (XRD and Raman), porosity (XRT), and microstructure (XRT) of the three-in-one composite before and after cycling were studied following the specifications described in this section. The experimental data were averaged from the three pellets prepared. Specific conditions for the study of each TCM were applied and are described in **Table 3**. Note that $MgSO_4$ was formulated from the hydrated form ($7H_2O$), while $MgCl_2$ composites were prepared from the anhydrous form to ease the manufacturing process as the hydrated form tends to overhydrate at ambient conditions.

The energy stored shown was calculated through both integrations by using the STA software and calculating the sensible heat and thermochemical heat. The latent heat stored (Q_{Latent}) was obtained by integrating the phase change peak in the STA software when cooling from 150 to 30 °C. The water sorption N is expressed as moles of water n_{H2O} sorbed per mole of anhydrous salt x (n_x), where x is magnesium sulfate and M_x is the molar mass of the anhydrous salt. When calculating the water sorption for the composite, where the content of TCM varies, the mass of the dehydrated was calculated from the TCM weight percentage in the host matrix. The thermochemical heat ($Q_{Thermochemical}$) was calculated by multiplying the moles of water lost (N), by the composite during dehydration [following Equation (4)], for the energy released per mole of water by the thermochemical material. The sensible heat from the composite was then calculated by Equation (5), where Q_{Total} is the total heat stored by the composite, Q_{Latent} is the heat stored by the PCM, and $Q_{Thermochemical}$ is the heat stored by thermochemical material.

$$N = \frac{nH_2O}{n_x} = \frac{mH_2O}{m_x} \cdot \frac{M_x}{MH_2O} \tag{4}$$

$$Q_{sensible} = Q_{Total} - \left(Q_{talent} + Q_{Thermochemical}\right) \tag{5}$$

The water uptake (W) and release at different temperatures steps were calculated from weight loss-gain during the STA analysis described above,[52] where the m_{H_2O} is the mass of water lost at the reaction time, m_x is the mass of the anhydrous, m_0 is the

initial mass, and m_t is the mass at the reaction time.

$$W(g/g') = \frac{mH_2O(t)}{m_x} = \frac{m_0 - m_t}{m_x} \quad (6)$$

The total conversion ($\chi(t)$) was calculated using the following equation,[53] where m_0 is the initial mass, m_t is the mass at the reaction time, and m_a is the final mass of the anhydrous

$$\chi(t)(\%) = \frac{m_0 - m_t}{m_0 - m_a} \times 100 \quad (7)$$

The energy density was calculated by using the total energy storage calculated and the density values for HDPE 0.93 g cm^{-3} (from the manufacturer), for the magnesium sulfate heptahydrate 2.66 g cm^{-3} (from the manufacturer) and calculating the density of the composite (e.g., 80/20) by the rule of mixtures. The cost was calculated using the value of HDPE from the manufacturer 2.5 and 80 £ kg^{-1} for the magnesium sulfate heptahydrate reported by Jarimi et al.[18]

Raman experiments were performed on the surface of the tablets before and after being cycled, at room temperature using a Renishaw confocal Raman microscope. The tests were performed with a solid-state laser of 785 nm (102–3200 cm^{-1}), exposure time of 10 s, and 50% of the laser power. 3 × 3 image mapping was used to scan the surface of the tablets (bottom and top) and a total of 27 points were measured.

A D8 Advance Plus X-ray powder diffraction (XRD) supplied by Bruker company (USA) equipped with an LYNXEYE detector using CuKα radiation ($\lambda = 1.5418$ Å) and θ–2θ geometry was used for the crystallinity analysis. For doing so, the pellet form of the sample was firstly ground to a powder form and then placed in the sample holder. Data were collected between 10° and 50° in 2θ with a step size of 0.02° and a counting time of 8 s per step. The X-ray diffraction patterns were recorded over-temperature stages to investigate the different crystalline phases when dehydrating the thermochemical material in pure form and the three-in-one composite. Two different programs were used once for chloride thermochemical materials up to 140 °C (to avoid side reactions and any damage to the equipment) and sulfates, nitrates, and carbonates materials up to 150 °C (see Table 3).

X-ray microtomography analysis was performed using the Skyscan1172 (from Bruker, Germany). This technique was used to study the open and closed porosity as well as the inner microstructure over 40 cycles. Before each set of scans, the rotation stage was aligned. Samples were scanned using 90 kV and 117 mA of source voltage and current, respectively, and were exposed to 280 ms during each snap. The scans covered 360 deg with a step of 0.2 deg, four frames were averaged, and the resultant project area was recorded for each rotation step. A 0.5 mm Ti filter was required. Cross-sectional and 3D images were reconstructed using NRecon software, where the ring effect and beam hardening were corrected. The misalignment was always kept between −10 and 10, as recommended for quantitative analysis.

6. Envision of the Hybridized Composite

The three-in-one concept was approached in two steps (see **Figure 2**); (1) the first step targeted the compatibility study between the components of the three-in-one at lab-scale, and (2) the second step aimed to further study the material's properties at a microstructural level. First, the compatibility between the TCM and the novel matrix working pairs was examined by five cycles stability study for 1 g tablets. Second, the working pairs that exhibited higher energy density and stability were studied using tablet sizes of 20 g and higher cycling times (40 cycles).

6.1. Part 1: Lab-Scale Study

In this section, the compatibility of the two components of the hybridized composite is studied and discussed. The lowest amount of novel matrix in the co-working matrix was tested for each of the proposed working pairs (90 wt% TCM/10 wt% matrix). With the eventual goal of assessing the working pair composition limitations and synergy between the working pairs (no side reactions, degradation, etc.). Thus, tablets of 1 g were prepared to contain 90 wt% TCM and 10 wt% of matrices, and tested in a humidity chamber over five cycles. Some of the working pairs failed at this stage as they presented chemical incompatibilities and/or structural problems, further explained in this section. The working pairs that did not show chemical incompatibilities or mechanical failure were reformulated with higher matrix content to investigate whether they could withstand the structure over a larger number of thermal cycles at the scale-up level.

6.1.1. Physical Stability

Among the matrices with storage potential, 90/10 formulation succeed for strontium bromide and magnesium sulfate working pairs (see **Table 4**). They show minor leakage (or none) and do not visibly break during cycling. MDI/$MgSO_4$ shows some leakage that can be reduced by increasing the ratio of SS-PCM in the composite. When it comes to magnesium chloride, they both require higher content of SSPCMs, given that the ratio 90-10 does not withstand even one cycle and they break and leak dramatically, whereas the ratio 80/20 samples show reasonable integrity after five cycles (see **Table 5**).

Interestingly, cellulose failed when combined with highly hygroscopic TCMs (tendency to undergo deliquescence) such as magnesium chloride. The intrinsic water absorption capacity of cellulose affects the sorption process of the TCM driving the system to deliquescence conditions. For strontium bromide and magnesium sulfate, cellulose can act as a matrix without interfering with the sorption processes; while this matrix does not provide additional energy storage capacity, it does allow stable, cost-extensive and pelletizes composites using a 10% weight of the matrix.

After preliminary tests with the 90/10 formulation, the working pairs were studied in the following ratios 90/10 and 80/20 with the ones that did not fail either chemically or mechanically and 80/20 and 75/25 for the ones that did not fail chemically. Thus, the experimental validation was conducted on the following working pairs: $MgCl_2$/MDI- $MgCl_2$/PEO-$MgCl_2$/HDPE ranging from 80/20 to 75/25, $SrBr_2$/MDI-$SrBr_2$/MDI- $SrBr_2$/PEO- $SrBr_2$/CLU and $MgSO_4$/HDPE-$MgSO_4$/MDI- $MgSO_4$/CLU both TCM working pairs ranging

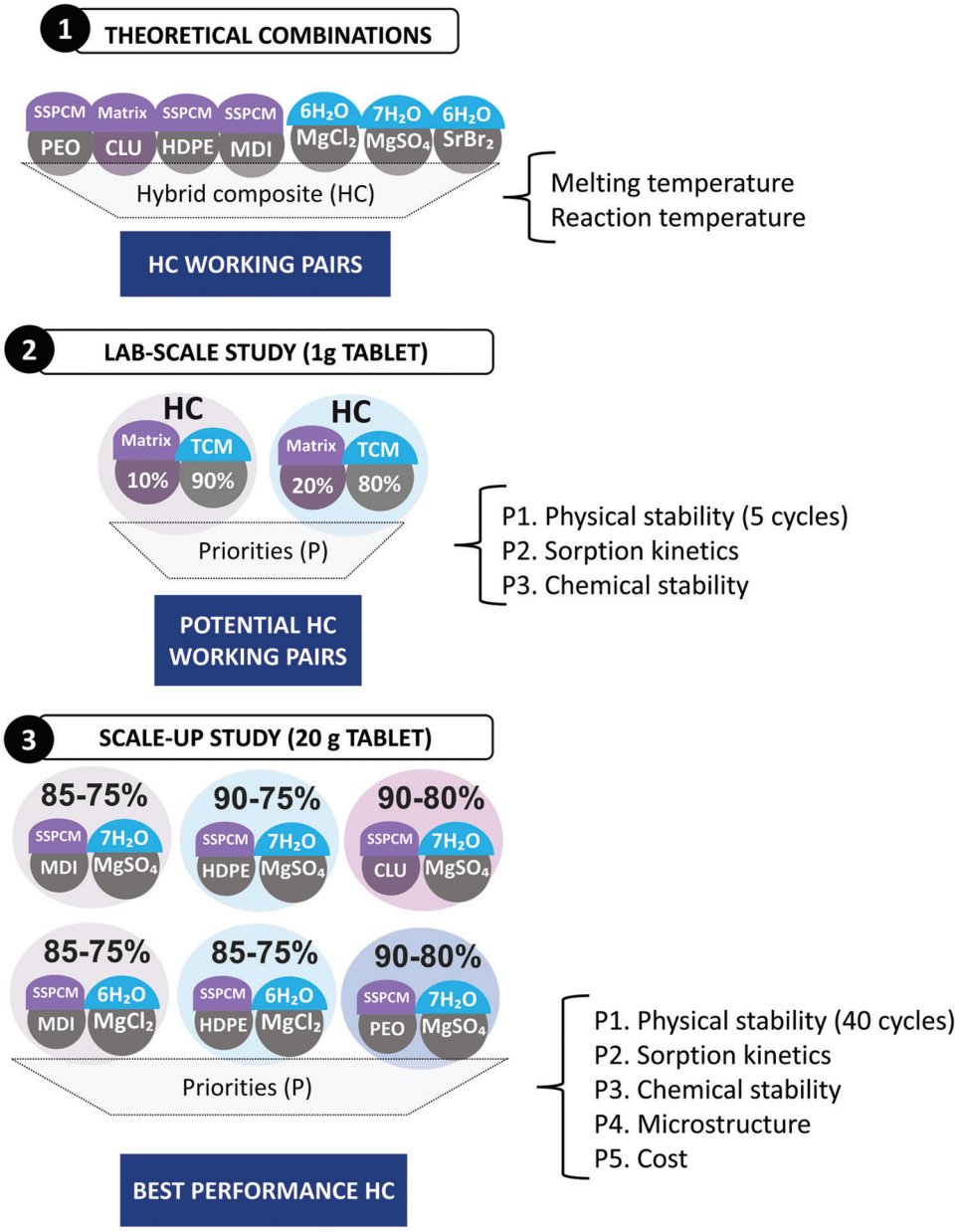

Figure 2. Mind map of the envision of the hybridized composite. 1) Theoretical combinations, 2) Lab-scale study, and 3) Scale-up study.

from 90/10 to 80/20. The study is described in the following section divided into: Section 6.1.2: Sorption process/energy stored (STA), and Section 6.1.3: Chemical stability (XRD).

6.1.2. Sorption Kinetics

To study the sorption process of the different working pairs, the hydration conversion time, hydration conversion, energy stored, and dehydration conversion were also calculated from the STA data (see **Figures 3** and **4**). Conversion rates range from 70% to 90% in most cases, but the relation is not proportional to higher TCM loading leading to higher reaction conversion. Magnesium sulfate has the highest energy stored reported by MDI 90/10 and HDPE 90/10, while conversions achieved by HDPE 80/20 and CLU 80/20 are close to the pure TCM (Figure 3). The hydration step (discharging) takes place at around 25–30 °C at a relative humidity from 60% to 80%, depending on pressure.[17,54] Since the hydration (≈25–30 °C) and the first dehydration stage (starting at ≈25 °C) overlap, the conversion from $MgSO_4{\cdot}7H_2O$ to $MgSO_4{\cdot}6H_2O$ occurs gradually when $MgSO_4{\cdot}7H_2O$ is formed. All working pairs show full hydration to the hexahydrate state, the experimental hydrated state achieved by magnesium sulfate after rehydration. While cellulose and MDI require 2.5 h to fully hydrate, HDPE composites need almost 3 h to complete hydration ≈96% (similar to the pure TCM). Higher content of PCM shows

Table 4. Images of the tablets after a five-cycle test of working pairs. The red squares show the failure of the test (major structural problems), while the ones in green showed decent physical integrity (minor or no changes).

	Solid-Solid PCM/Alternative matrix (TCM %wt./matrix %wt.)				
TCM	**None**	**PEO**	**HDPE**	**MDI**	**Cellulose**
Magnesium sulphate		-	 90/10	90/10	 90/10
Strontium bromide		90/10	-	 90/10	 90/10
Magnesium chloride		 80/20	 80/20	 80/20	-

Table 5. Cycling outputs of the $MgSO_4$/HDPE working pairs studied in the scale-up section for 1, 5, 15, 25, and 40 cycles. Note that samples in green are considered suitable for the validation study, while samples in red are discarded.

Working pair (TCM/Matrix)	Cycles	A-90 wt.% /10 wt.%	B-85 wt.% /15 wt.%	C-80 wt.% /20 wt.%	M-75 wt.% /25 wt.%
$MgSO_4$/HDPE	1 cycle				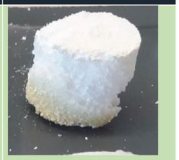
	5 cycles				
	15 cycles	X		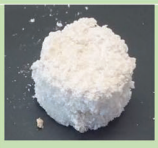	
	25 cycles	X			
	40 cycles	X			

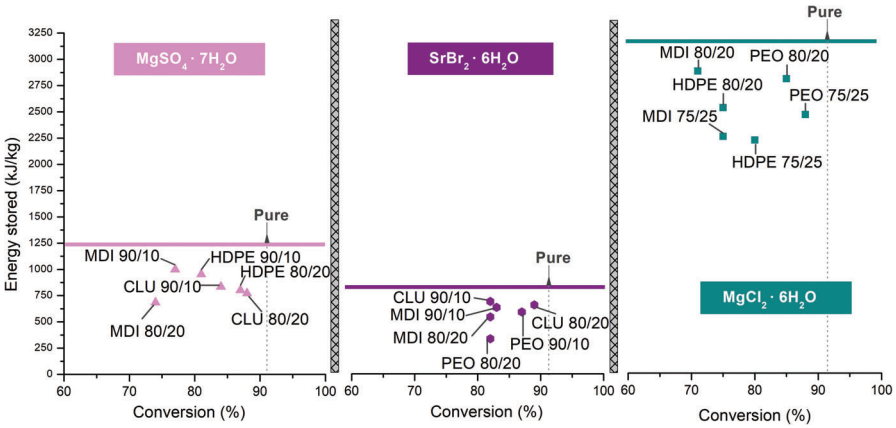

Figure 3. Dehydration conversion and enthalpy of fusion for the formulation containing 80 wt% TCM/20 wt% matrix (80/20), 90 wt% TCM/10 wt% matrix (90/10), and 75 wt% TCM/25 wt% matrix (75/25) at the different test conditions; for magnesium sulfate 25–150 °C at 1 °C/min-60 min hold, for strontium bromide 25–90 °C at 1 °C/min-60 min hold; and for magnesium chloride 25–140 °C at 1 °C/min-60 min hold in the STA. Pure PCM data are illustrated with a flat line for the energy stored and a dotted line for the conversion.

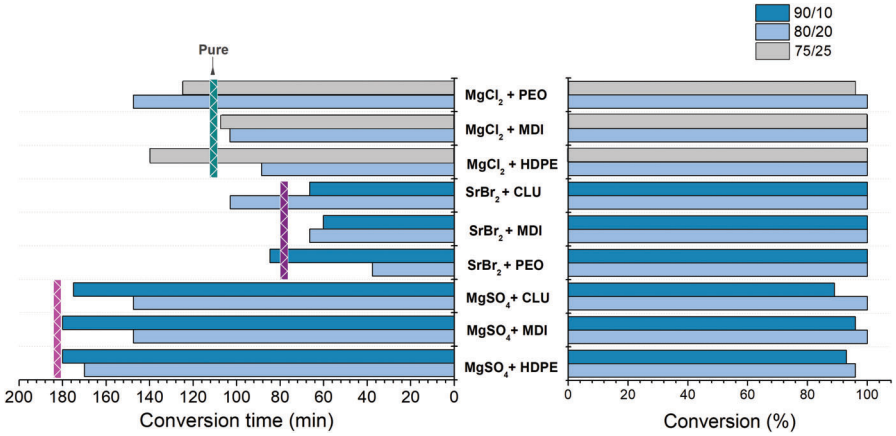

Figure 4. Hydration conversion and hydration conversion time for the formulation containing 80 wt% TCM/20 wt% matrix (80/20), 90 wt% TCM/10 wt% matrix (90/10), and 75 wt% TCM/25 wt% matrix (75/25) at the different conditions; for magnesium sulfate 3 h at 30 °C-80% R.H., for strontium bromide 2.5 h at 30 °C-50% R.H.; and for magnesium chloride 2.5 h at 40 °C-30% R.H. Note that the initial magnesium chloride sample was anhydrous, thus these values are for the second hydration of the composite. Pure TCM conversion time is illustrated with a vertical line; green for magnesium chloride, purple for strontium bromide, and pink for magnesium sulfate.

to facilitate hydration as higher conversion rates are achieved at lower times. Strontium bromide working pairs are the ones that store the lowest energy, with cellulose 80/20 and 90/10 being the highest energy of the $SrBr_2$ working pairs. PEO 80/20 is the PCM pair that leads to lower energy, while 90/10 appears to be an optimal formulation with a similar conversion rate as pure TCM. Strontium bromide working pairs show the shortest hydration times given their high reaction rate.[55] Under the same conditions, pure strontium bromide hydrates in 80 min while 90/10 MDI, PEO and CLU hydrate faster (≈60 min) (see Figure 4). Therefore, it is proved that the PCM matrix can help the sorption process allowing faster reaction times. Magnesium chloride has an intrinsic high energy storage capacity, although this is reduced by the addition of PCM. Some of the working pairs still present a large energy density compared to the others studied, such as MDI 80/20 and PEO 80/20. As with the other TCMs, the higher the content of TCM the higher the energy stored by the $MgCl_2$ three-in-one composite. From the SS-PCMs, PEO based are the ones that show higher conversion while MDI is the lowest one. In general, higher amounts of PCM lead to higher conversion rates, thus, better desorption values, but lower energy stored. Regarding hydration, 80/20 shows lower hydration times than the pure TCM for MDI and HDPE. All the working pairs are hydrated after 2.5 h, being 80/20 HDPE the fastest (88 min), whereas pure magnesium chloride hydrates in 124 min.

6.1.3. Chemical Stability

The chemical stability was studied using a high-temperature X-ray diffraction apparatus, each TCM working pair was subjected to a different temperature program according to their nature. The dehydration conditions from 25 to 120 °C in the case of strontium bromide, magnesium chloride from 25 to 140 °C to avoid secondary reactions, and magnesium sulfate from 25 to 150 °C. The XRD patterns, at the highest test temperature, were recorded after a 30 min isotherm to ensure the stabilization of the crystalline

phase. The patterns of the pure TCM sample are also shown for comparison purposes (figures are included in the Supporting Information). This technique is used to check that no other crystalline phases are present in the composite after dehydration and that the species obtained from the hydrated to dehydrated form are the same as the pure material ones. For that reason, just the working pairs containing the highest PCM (80/20 for $MgSO_4$ and $SrBr_2$, and 75/25 for $MgCl_2$) percentages are characterized. The results obtained are discussed for each TCM.

Pure magnesium sulfate dehydrates in three different steps, from hepta to hexa in the range from 25 to 40 °C; the hexahydrate form is stable up to 70 °C when the transition from hexa to an amorphous monohydrate form takes place up to a temperature range of 150 °C as also reported by Ferchaud et al.[56] HDPE and cellulose working pairs show similar behavior as the pure TCM, the amorphous phase appears at 70 °C. From 70 to 120 °C just two visible crystal diffraction peaks from HDPE can be seen around $2\theta = 21.6°$ and 23.8°.[47] Above 120 °C HDPE is melted and no peaks are reported. MDI working pair shows interesting results as the amorphous phase is in this case delayed to appear at higher temperatures, while a new hydrated form can be seen in the XRD patterns $MgSO_4 \bullet 4H_2O$. In light of the results, this was repeated to prove the validity of this data, which was confirmed by a second test. This form has not been reported in the literature as a natural form of magnesium sulfate but it is just achieved by synthetic processes.[57] The tetrahydrate is formed at 90 °C, where normally the amorphous phase would be formed. At 120 °C, the amorphous phase appears to coexist with the tetrahydrate as the intensity of the peaks lower. The amorphous phase is then seen at 150 °C when the TCM has completely dehydrated. This evidences that PCM matrices can affect and change the dehydration steps followed by the TCM and might stabilize forms that are not naturally stable within the PCM structure. Another hypothesis is that given the melting point of the PCM (MDI), around 50–60 °C, this process interacts with the desorption reaction through the heat involved in the phase change as the dehydration from hexa to mono starts (55–60 °C), which may affect the reaction rate/kinetics of the TCM.

Strontium bromide dehydrates in two steps, firstly from 25 to 40 °C to the hexahydrate form, then at ≈60 °C, a transition from hexa to mono starts and the form is stable up to 120 °C (see Figure S1, Supporting Information), which is in good agreement with the literature.[58] Unlike magnesium sulfate, the strontium bromide TCM/PCM working pair shows similar XRD patterns as the pure TCM. The interaction between TCM and PCM is a factor that determines the effect seen for magnesium sulfate and MDI. The difference in peak intensities can be attributed to a modification of the grain size in the powder sample as reported for other TCMs.[56]

The dehydration reaction of $MgCl_2 \bullet 6H_2O$ until 150 °C performed at 1 °C min^{-1} was reported to present two dehydration steps with the formation of the crystalline phases $MgCl_2 \bullet 4H_2O$ in the temperature range of 80–110 °C and $MgCl_2 \bullet 2H_2O$ in the temperature range of 120–140 °C, as described by Ferchaud et al.[56] The XRD patterns obtained in this study show a slightly earlier transition from $MgCl_2 \bullet 4H_2O$ to $MgCl_2 \bullet 2H_2O$ phase, given that the tetrahydrate phase is detected already at 70 °C, see the figures in the Supporting Information. The same heating rate and XRD program conditions have been used, thus this might be attributed to the atmosphere as we operate under open air and the authors worked under controlled partial vapour pressure of 13 mPa atmospheres. Besides, no XRD peaks characteristic of the crystalline phase of magnesium hydroxy chloride MgClOH has been observed on the spectra at 140 °C after 30 min, therefore no side reaction or decomposition is seen. TCM/PCM formulations crystalline peaks sequence is modified for the MDI and PEO composites. In both cases, the $MgCl_2 \bullet 6H_2O$ phase is formed up to 70 °C, and the crystalline phase of $MgCl_2 \bullet 4H_2O$ is formed at 80 °C as reported by Ferchaud et al.[56] In both cases, the intensity of the peaks is very low, and the intensity of the peaks dramatically changes before the dehydration from hexa to tetra. This phenomenon was also reported by Ferchaud et al.,[56] who attributed this to a preferential orientation change of the material during the measurement. The same explanation for the phenomena observed in the magnesium sulfates pairs can be applied in this case, regarding the tetrahydrate formation temperature shifts. The two plausible hypotheses are that (1) the latent heat reaction can affect the sorption reaction by shifting the crystalline phase formation or (2) the polymeric structure can affect the crystalline phase transformation driving a shift in the transition from one crystalline phase to the other one.

6.2. Part 2: Scale-Up Study

In the previous section, the hybridized composite was proven to be stable for up to five thermal cycles. Aiming to transit to the next manufacturing level, the set of working pairs that exhibited higher energy density are evaluated at a scale-up level after 40 cycles. The TCMs selected for the scale-up study were magnesium sulfate heptahydrate ($MgSO_4 \cdot 7H_2O$) and magnesium chloride ($MgCl_2 \cdot 6H_2O$). This section presents the results of the cycling cycles following a throughout characterization of the 20 g composites.

Given the large number of samples considered in this section, a nomenclature code has been assigned. The sample is assigned a letter, e.g., 90 wt% $MgSO_4$/10 wt% HDPE is the letter A, whereas the cycling stage is identified by a number, e.g., 1 cycle is number 1, which are indicated in the following **Tables** 5 and **6**. Regarding the cycles, sample A cycled once would be A1, A5 for 5 cycles, A15 for 15 cycles, A25 for 25 cycles, and A40 for 40 cycles. From this section until the end of the paper, this nomenclature will be followed to refer to the samples in the scale-up study section.

6.2.1. Physical Stability

Magnesium sulfate working pairs stand up as the most promising candidates for the hybridized composite as they can withstand up to 40 cycles without showing major leakage, breakage or chemical degradation (see Tables 5 and 6). Among the SSPCM working pairs, MgSO4/HDPE shows the best compatibility as well as physical integrity over cycles for either 80% wt, 85% wt, or 75% wt formulations (see Table 5). These results are in good agreement with the paper previously published[3] and prove that using a larger tablet size does not affect, cycling stability-wise or the synergy between magnesium sulfate and HDPE. However, a slight degradation rate is observed on the surface of the tablet, not

Table 6. Cycling outputs of the $MgSO_4$/MDI and $MgSO_4$/CLU working pairs were studied in the scale-up section for 1, 5, and 15 cycles. Note that samples in green are considered suitable for the validation study, while samples in red are discarded.

Working pair (TCM/Matrix)	Cycles	-	J-85 wt.%/15 wt.%	K-80 wt.%/20 wt.%	L-75 wt.%/25 wt.%
$MgSO_4$/MDI	1 cycle	-	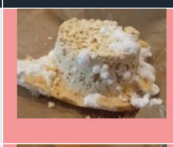		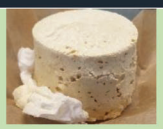
	5 cycles	-		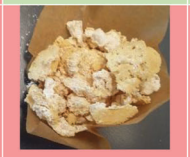	
$MgSO_4$/CLU	Cycles	D-90 wt.%/10 wt.%	E-85 wt.%/15 wt.%	F-80 wt.%/20 wt.%	-
	1 cycle		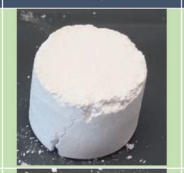		-
	5 cycles	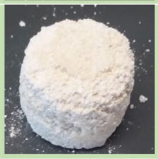	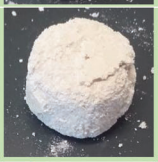		-
	15 cycles	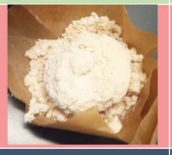			-
$MgCl_2$/HDPE	Cycles	-	N-85 wt.% /15 wt.%	O-80 wt.% /20 wt.%	P-75 wt.% /25 wt.%
	1 cycle	-			
	5 cycles	-	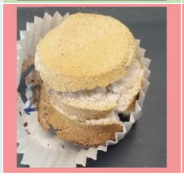		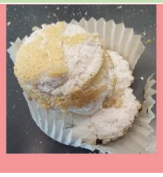

the inside, which is due to the lower surface-over-volume ratio. Whereas sample M (75/25) does contract throughout the thermal cycles, samples B and C keep their tablet shape after cycling. The working pair containing MDI shows leakage after one cycle and major breakage after five cycles, concluding that MDI polymer, unlike HDPE, does not work as a supporting matrix for the three-in-one system. This might be due to the MDI acting as a hard segment (using as an analogy a polymer blend) not allowing mobility and restructuring of the TCM in the composite after one cycle not providing a contained-flexible structure, which leads to leak-

Table 7. Cycling outputs of the $MgSO_4$/MDI and $MgSO_4$/PEO working pairs were studied in the scale-up section for 1, 5, and 15 cycles. Note that samples in green are considered suitable for the validation study, while samples in red are discarded.

$MgCl_2$/MDI	Cycles	-	Q-85 wt.% /15 wt.%	R-80 wt.% /20 wt.%	S-75 wt.% /25 wt.%
	1 cycle	-	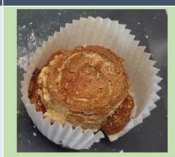		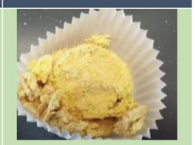
	5 cycles	-			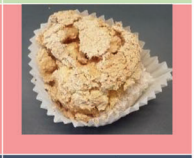
$MgCl_2$/PEO	Cycles	-	T-85 wt.% /15 wt.%	U-80 wt.% /20 wt.%	V-75 wt./% 25 wt.%
	1 cycle	-	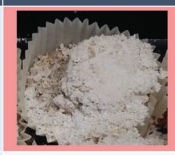		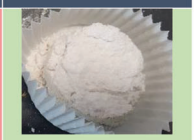
	5 cycles	-	X	X	

age of the PCM; and after five cycles resulting on the collusion of the structure (breakage). In this case, a polymer-based blend (e.g., PEG-MDI) could be an alternative to improve behavior.[29,59]

Regarding magnesium chloride working pairs, all the formulations studied were not able to withstand more than five thermal cycles, some of them broke just after one cycle, like the ones containing PEO and MDI. Increasing the size of the tablet in this case, leads to major leakage issues from the bottom part of the tablet, as seen in the images from **Table 7**. A noticeable difference between magnesium sulfate and magnesium chloride working pairs lies in the intrinsic lower viscosity of magnesium chloride when melting, which adds another challenge to finding a suitable PCM that can synergistically work as a co-matrix and that keeps the composite structure. Thus, given the poor physical integrity over cycles, magnesium chloride candidates are discarded for further experimental validation.

6.2.2. Sorption Kinetics

The dehydration conversion of samples after 1 and 40 cycles are compared in **Figure 5**; the reaction rate at the highest conversion rate is also shown in the graph. The conversion rate appears to be slightly higher at larger cycling stages, as demonstrated in the previous section. The hybridized composite reaches a stable structure over cycles that enable hydration/dehydration processes in the TCM/Matrix structure. The dehydration process

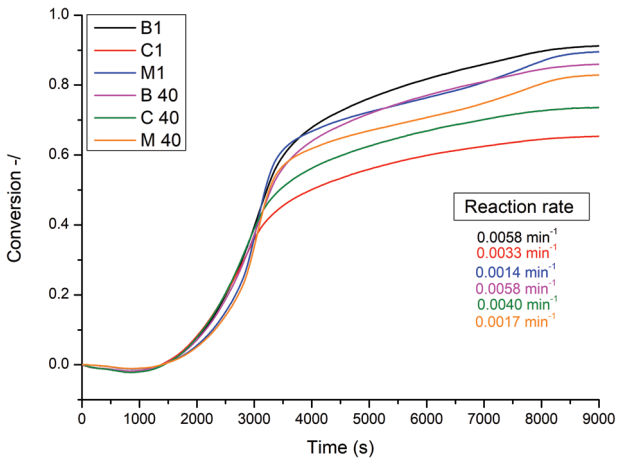

Figure 5. Dehydration conversion versus time of the samples containing HDPE (B, C, M) for one cycle (1) and 40 cycles (9) in the right figure. Note that the data are averaged from two sets of measurements. STA program from 25 to 150 °C at 1 °C/min-hold 60 min. The average reaction rate is calculated in the graph following Equation (4) in the Experimental Section.

consists of multiple dehydration stages, which involve the loss of 5 mols of water from hexahydrate to monohydrate from 25 to 150 °C.

The conversions values range from 80% to 97% for the HDPE working pairs. As stated, the dehydration step of epsomite (from

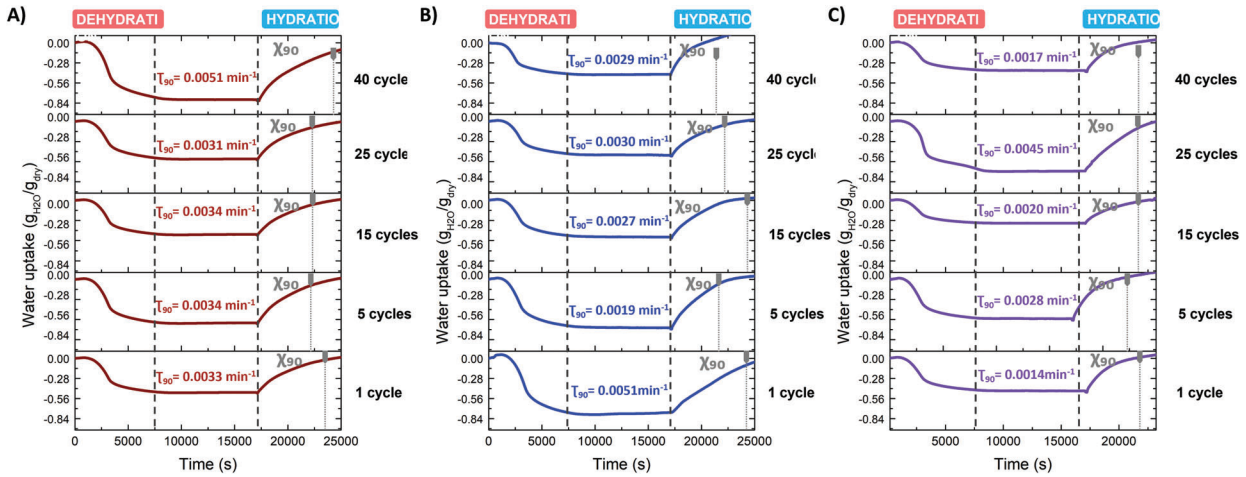

Figure 6. A) Water uptake of the 85 wt% $MgSO_4 \cdot 7H_2O$ and 15 wt% HDPE (hydration/dehydration); B) water uptake of the 80 wt% $MgSO_4 \cdot 7H_2O$ and 20 wt% HDPE (hydration/dehydration); and C) water uptake of the 75 wt% $MgSO_4 \cdot 7H_2O$ and 25 wt% HDPE (hydration/dehydration). Note that the data are averaged from two sets of measurements. STA program from 25 to 150 °C at 1 °C/min-hold 60 min; hydration at 30 °C 80% R.H. for 2.5 h. The reaction rate at 90% conversion was calculated for each working pair, following Equation (4) in the Experimental Section.

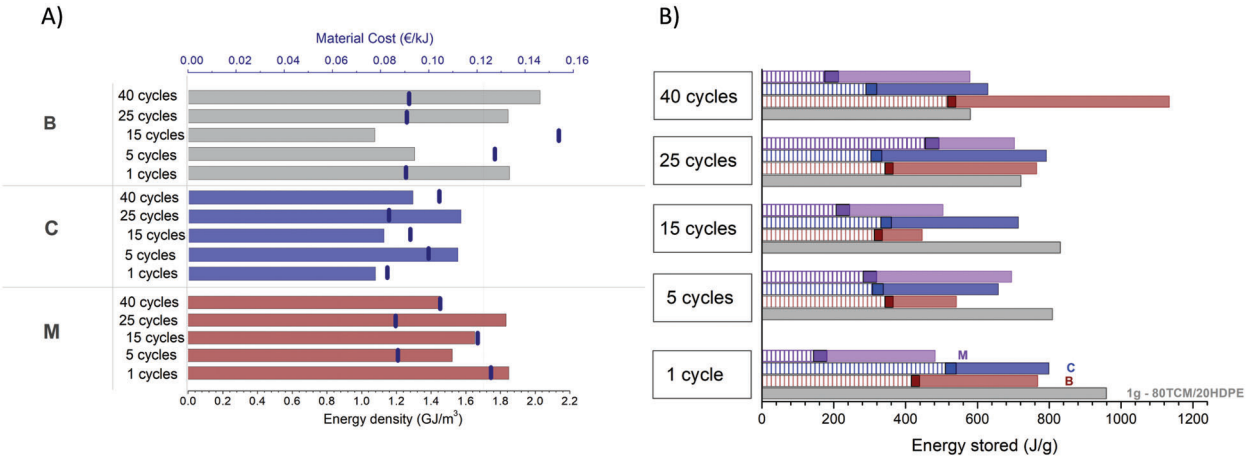

Figure 7. A) The three-in-one energy density (GJ m^{-3}) and material cost (€ kJ^{-1}) of B, C, and M formulations. B) Energy density stored by component (from left to right; sensible, latent, and thermochemical) for the 1 g-80 wt% TCM/20 wt% matrix, B, C, and M.

hexa to hepta) is complex and can be described as a deceleration reaction controlled by interface advancement[60] as we can see in Figure 5. Ruiz-Agudo et al.[60] also observed that during the latest stages of the reaction a reduction in the reaction rate when adding additives into pure Epsomite, among them polyacrylamide acid, which was associated with the obstruction of the diffusional removal of the gaseous product by the surface product layer and the stronger bonding of H_2O molecules in lower hydrates.

Comparing the hydration curves of 1 and 20 g tablets, similar behavior can be seen with conversions of 90% for the hydration reaction in less than 2.5 h (pure TCM needs 3 h to fully hydrate), see Figure 6. However, 20 g tablets show larger hydration times (114–180 min) than 1 g tablets (70–150 min). Comparing the 40-cycled composites in the tablet form to the one-cycled samples, the 40-cycled one takes longer to reach χ_{90} (90% conversion). This might be because the microstructure created by the polymer and the thermochemical material takes some cycles to stabilize, which is key to allowing for a higher and more steady conversion rate. The powders rapidly agglomerate when dehydrating, hindering water absorption and reducing the conversion rate. Hence, the structure created by the polymer and the thermochemical material is key to allowing a high conversion rate (**Figure 6**).

The energy stored by the working pairs is illustrated in **Figure 7**A,B. The sample B5 (85 wt% $MgSO_4 \cdot 7H_2O$ and 15 wt% HDPE) cycled 40 times, is the one that shows higher energy storage, 1120 kJ kg^{-1}, higher than pure TCM. The 20 g tablet $MgSO_4$/HDPE working pairs are also compared to the 80/20-1 g reported in the previous paper.[3] Scaling up the composite has an expected influence on its conclusion that the energy stored by the 20 g tablets is higher after 15 thermal cycles and the energy density reaches values up to 2.1 GJ m^{-3}. The cost of the material per energy stored is slightly higher for B-15 cycles.

6.2.3. Chemical Stability

$MgSO_4$/HDPE XRD patterns from 25 to 150 °C are very similar to the ones reported by pure magnesium sulfate after the first dehydration/hydration cycle, as well as the absence of low hydrated magnesium sulfate phases (e.g., less than 6 mol H_2O per mol $MgSO_4$).[61] Interestingly, the XRD patterns of the samples after cycling (1, 15, and 40 cycles) reveal that a portion of the TCM material converts into kieserite, the crystalline structure of $MgSO_4{\cdot}1H_2O$[61,62] above 70 °C, instead of fully converting into the monohydrate amorphous structure as reported in the literature[56] and like the powder samples characterized. Such structure has been reported to be synthetically formed at specific and controlled pressure and temperature conditions.[63] Kieserite is a monoclinic structure, while HDPE, which has a crystallinity of up to 80%, can be found in orthogonal and monoclinic cells.[64] Tetragonal, orthorhombic, and monoclinic phases are only slight distortions of the cubic structure.[65] Besides, the selection of nucleating agents mainly follows the rules proposed by Telkers that nucleating agents must have less than 15% variation in the unit cell from the existing structure.[66] Thus, given their crystal structure similarities, they could act as nucleation agents when present in small percentages in the main crystalline structure (monoclinic or orthorhombic in this case) and favour the partial formation of the crystalline monohydrate phase. Even though, the amorphous phase is still present as confirmed by the XRD patterns (note that $MgSO_4{\cdot}1H_2O$* refers to patterns with a noticeable content of amorphous phase). Therefore, a percentage of the TCM might follow the route (1) from hexahydrate to monohydrate monoclinic and another portion route (2), from hexahydrate to monohydrate amorphous. The intensity of kieserite varies within the XRD patterns, which denotes that the ratio amorphous/crystalline phase is heterogeneous throughout the tablet TCM/PCM content. Besides, a tendency to an increasing crystallinity content over cycles is observed in the XRD patterns from 1 to 40 cycles as the intensity of the peaks is higher and wider X-ray scattering profiles from the amorphous phase can be seen.

While in the literature the formation of the amorphous phase has been related to slow reaction rates at pressures <13 mbar, in the three-in-one system this seems to be partially tackled by the addition of HDPE, which favours the reorganization of the crystal structure to monoclinic. Along with this, HDPE appears to recrystallize into the initial structure not increasing the amorphous content within the polymer structure as seen in the X-ray diffraction patterns (see figures in the Supporting Information). The crystal diffraction peaks from HDPE can be seen at 2θ = 21.6° and 23.8° up to 120 °C, they disappear at 150 °C due to the melting of the polymer and reappear given the recrystallization at 25 °C after cooling down.

Once the monohydrate crystalline phase has been identified in the XRD patterns, the conversion rates for hydration and dehydration as the rehydration from kieserite are studied and compared with the values from the amorphous phase. However, as reported by Steiger et al.[61] the complete conversion to hexahydrite was rapidly achieved at 65%, 70%, 75%, and 80% RH, which are within the hydration conditions of this study. Besides, the hydration of $MgSO_4{\cdot}H_2O$ (kieserite) and the formation of $MgSO_4{\cdot}6H_2O$ (hexahydrite) were defined as kinetically hindered. The authors found out that above the deliquescence humidity of kieserite, the reaction proceeds via a two-stage reaction pathway involving the dissolution of kieserite and the subsequent crystallization of hexahydrite from a highly supersaturated solution.[61] Therefore, the initial hexahydrite state can be reached for both amorphous and crystalline monohydrates.

Raman spectroscopy was used as a complementary technique to X-ray diffraction. A mapping of the bottom (part in contact with the tray) and top (part in contact with the environment) surfaces of the tablets was conducted to 1- and 40-cycles samples. Kieresite, hexahydrite, and HDPE peaks were identified, the following references were used to identify the peaks; Wang et al.[67] for magnesium sulfate species and Ibrahim et al.[68] for HDPE. The hydrated magnesium sulfates could just be identified in the spectral region of SO_4 fundamental vibrational modes, given that the Mg-sulfates peaks are in the spectral region of water OH stretching vibrational modes.

A colored mapping of the surface is provided for $MgSO_4$-HDPE working pairs in **Figure 8**A–C. From the 27 points measured in different locations of the tablet surface, one can conclude that HDPE has a higher concentration at the bottom of the tablet, an effect that is aggravated over cycles. This might be given to the higher viscosity of HDPE in comparison to magnesium sulfate. While magnesium sulfate remains "static" in the structure, HDPE has mobility and flows when melting, which leads to an apparent higher content of polymer in the bottom of the tablet. However, this cannot be quantified by the Raman technique. Besides, amorphous content can be observed as the patterns present a tendency to the Boson peak,[69,70] which is characteristic of non-crystalline or semicrystalline structures (amorphous HDPE content). Again, the monohydrate crystalline phase has also been identified in the hydrated tablet, which confirms that part of the hexahydrite is converting into kieserite. This data indicates that a percentage of kieserite might not be transforming to hexahydrate and remain in the lattice structure of the magnesium sulfate hexahydrate as the crystalline monohydrate, which could lower the reaction rate and conversion.

6.2.4. Microstructure and Porosity (XRT)

The reconstruction of the microstructure images provided by X-ray tomography is shown in **Tables 8–10**. Samples containing HDPE exhibit a hole-like shape right in the middle of the tablet (see Table 8), this effect is even more pronounced with higher TCM content and a larger number of cycles. While B1 and C1 do not show the hollow region when increasing the number of cycles (B5 and C5), this region appears to be larger and does not grow further up to 40 cycles. Both working pairs maintain the tablet's physical dimensions (diameter and thickness) even after 40 cycles. This can be correlated to the porosity values obtained (see **Figure 9**) when at 25 cycles the porosity reaches a constant value, as also reported in the previous study.[3] A higher percentage of PCM (20–25 wt%) increases the TCM/PCM contact area, which provides a skeleton to keep the TCM in "static" positions in the composite. While a lower percentage of the polymeric PCM (10–15 wt%) is not enough to provide enough contact area and retain the structural stability, leading to the TCM's particle agglomeration, which might be the driving force to form the hollow

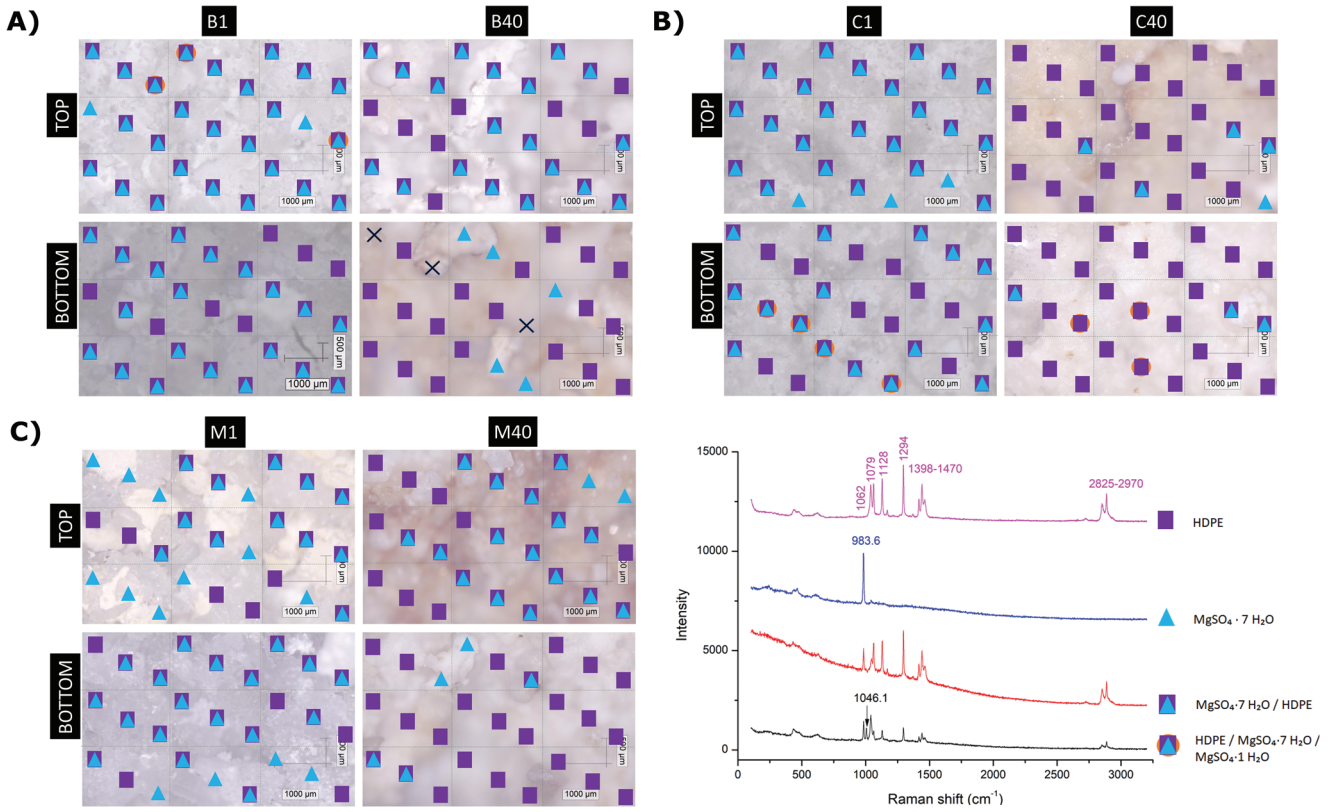

Figure 8. Raman 3 × 3 mapping images (bottom and top) with scanned points identified, following legend on the graph (D); A) B1 and B405 samples, B) C1 and C40 samples, and C) M1 and M40 samples.

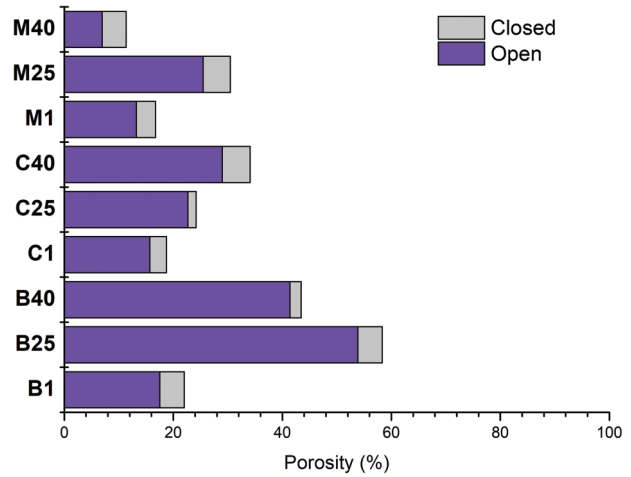

Figure 9. Open and closed porosity percentages were calculated through the XRT reconstruction in the 2D model for the $MgSO_4$/HDPE working pairs.

region. Excess on the polymer content would reduce the porosity requirements and hence difficult the water vapour transport (due to low porosity of 11%–27%). As an example, the 25 wt% of HDPE composite shrinks to almost a third of the initial diameter after the thermal cycles.

6.2.5. Interaction between TCM and PCM

The heating profile of the hybrid composite is shown in **Figure 10**, as seen in the figure there are four peaks that correspond to the four chemical [(1) to (4) in the graph] and physical processes taking place within the composite upon heating and cooling; (1) dehydration of thermochemical material, (2) melting of PCM, (3) solidification of PCM, and (4) hydration of thermochemical material.

The presence of the thermochemical material affects the crystallization process of HDPE, its crystallinity degree as well as the nucleation mechanism. The heat flow curves for the heating and cooling of HDPE in the $MgSO_4$-HDPE composite (B1, C1, and M1) are shown in Figure 10, HDPE crystallizes even after 40 heating cycles. Comparing the heating and cooling curves nonsignificant subcooling effect can be observed, ± 2 degrees of difference, which is within the error associated with the measurements of the equipment and the different heating rate, 1 °C min^{-1} and cooling rate 2.5 °C min^{-1}. Besides, pure HDPE shows a melting point onset of 125–127 °C and peak at 130–132 °C, while in the hybridized composite the melting peak of HDPE is wider and shifted to lower temperatures with an onset of 110 °C. This might be attributed to the chemical-physical effect of the TCM in contact with the polymer, the TCM particles undergoing a chemical process with the heat involved in the reaction, might act as a hot point for the HDPE to melt at lower temperatures. As reported by Seven et al.,[71] during nucleation the polymer HDPE

Table 8. XRT reconstruction images of samples B1, B5, and B9 from top to bottom of the tablets.

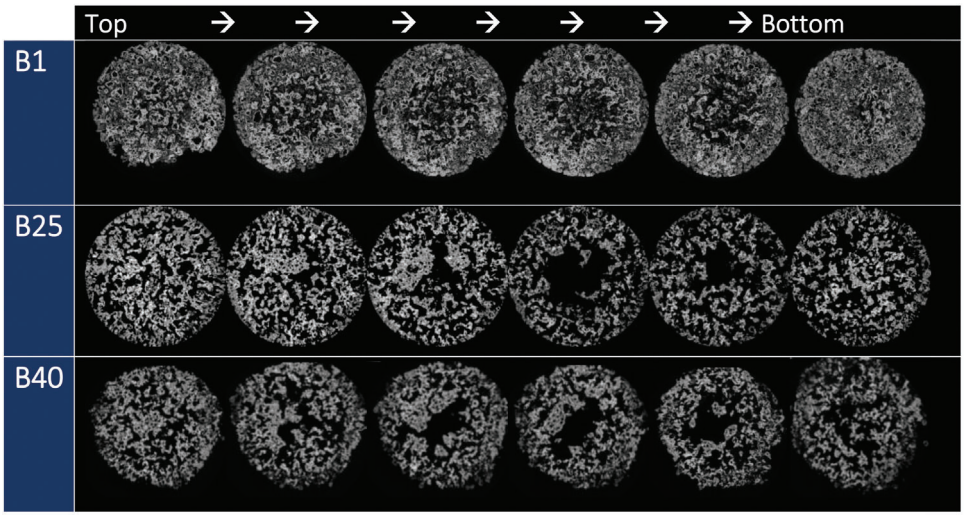

Table 9. XRT reconstruction images of samples C1, C5, and C9 from top to bottom of the tablet.

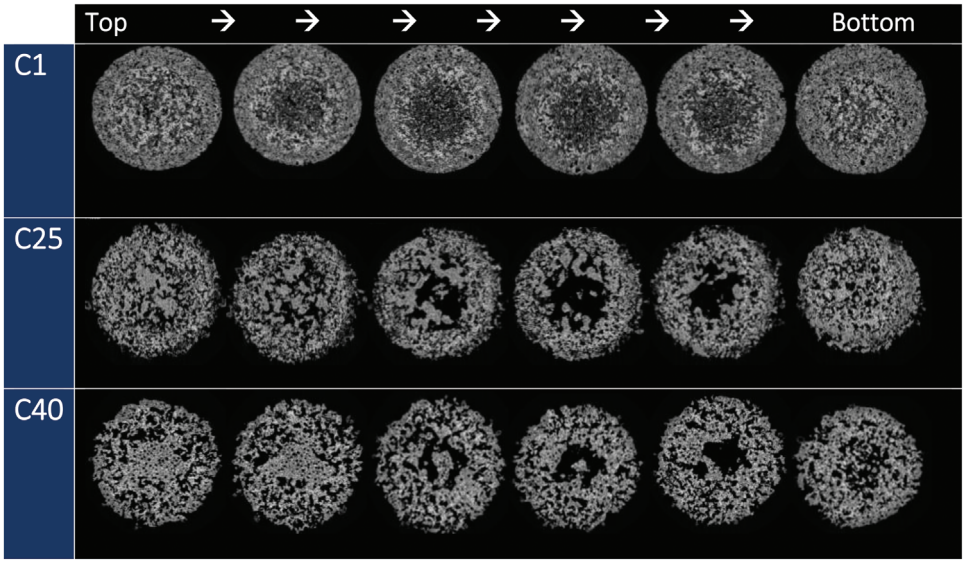

undergoes a phase change upon cooling where chains orient and align at the molecular scale into a periodic lattice. During crystal growth, polymer chains orient around the initial nucleation site, or nucleus, in a 3D pattern most often forming a spherical crystal cluster called a spherulite. Complete crystallization occurs when the crystalline and noncrystalline domains become space-filling.

7. Conclusions

In this paper, novel matrices for sorption thermochemical materials have been proposed to tackle the current challenges in thermochemical storage materials synthesis and manufacturing. Three sorption-based TCMs (strontium bromide, magnesium sulfate, and magnesium chloride) and three SS-PCMs (MDI, PEO, and HDPE) and one matrix (cellulose) were combined to design a working pair set of formulations.

Among the working pairs studied, magnesium sulfate stands up as the best TCM candidate. Magnesium chloride working pairs showed major leakage and breakage issues just after five cycles. Magnesium sulfate formulations experimentally validated serve as a scale-up study from 1 to 20 g to consolidate the potential of the hybridized matrix. The polymer working pairs showed high energy storage capacity of up to 2.4 GJ m^{-3}. Besides, high

Table 10. XRT reconstruction images of samples C1, C5, and C9 from top to bottom of the tablet.

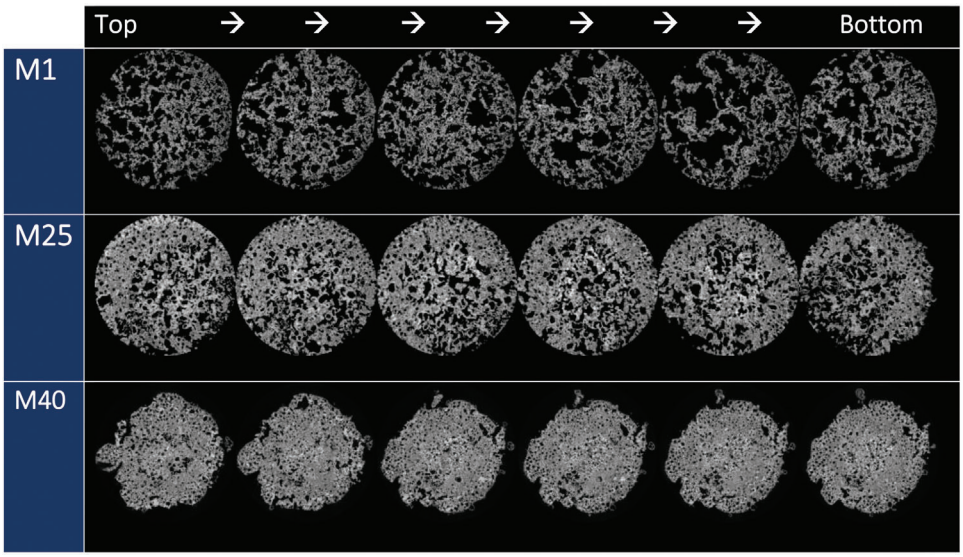

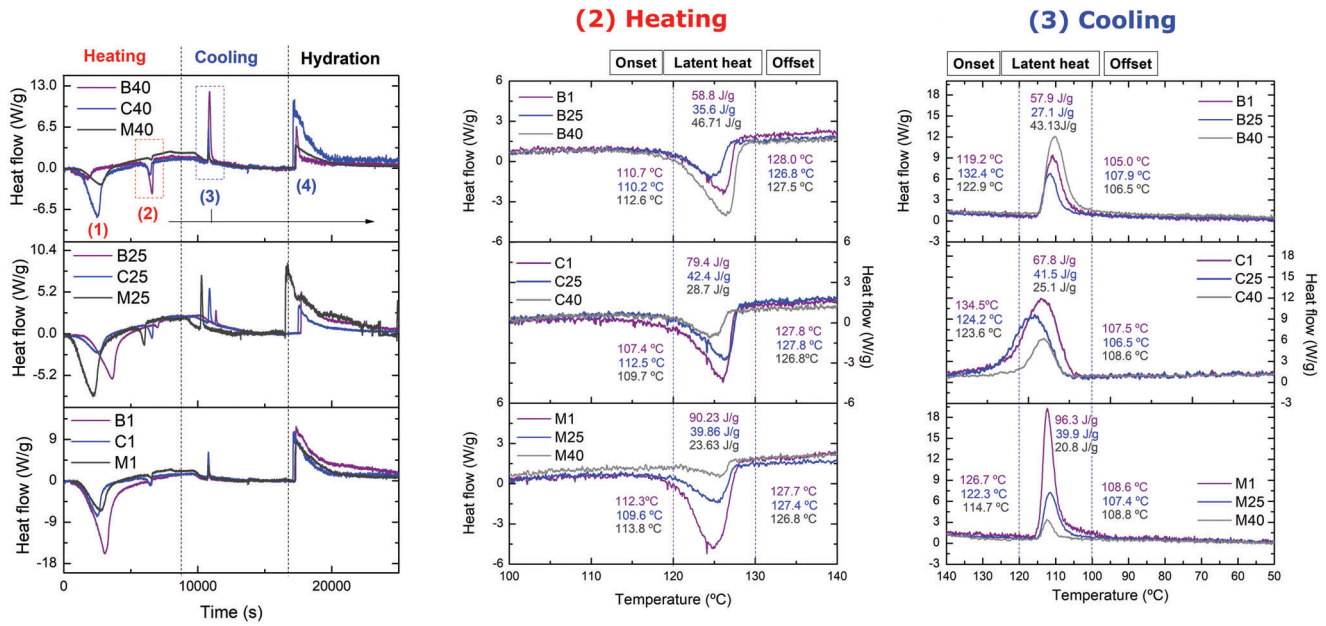

Figure 10. Heat flow versus time (left image) of the initial samples after one cycle B1, C1, and M1, where (1) dehydration of TCM, (2) melting of PCM, (3) solidification of PCM, and (4) hydration of TCM; and heat flow versus temperature on the right; (2) melting and (3) solidification curves of the PCM component in the hybrid composite for B, C, and M after 25 and 40 cycles HDPE melting peaks. Heating from 25 to 150 °C 1 °C/min-hold 30 min, cooling from 150 to 25 °C at 2.5 °C min^{-1}.

dehydration (70%–95%) and hydration conversions (90%) were reached even after 40 thermal cycles while maintaining structural integrity. A 25–20 wt% of HDPE was set as optimal for the $MgSO_4$-HDPE working pair, providing a compromise between energy stored, porosity, and mechanical integrity. The phase change material was found to act as a nucleating agent in the magnesium sulfate crystallization process forming a synthetic monohydrate crystalline phase (Kieserite) instead of the reported in the literature monohydrate amorphous phase. Cellulose exhibits good results after a few cycles but over further cycles, the structure collapsed and failed, which proved that a backboned structure might be needed for its practical implementation.

Interestingly, this study has explored the effect of adding different matrices into thermochemical material from a different perspective. Generally, the evaluation of TCM matrices is driven by sorption kinetics, energy stored and structural stability. In this

study, the authors have also observed the effect of matrices on the crystal structure of TCM and their morphological changes through charging/discharging processes. The effect of the matrix has been proved to induce certain structural deformation or changes not observed in the pure TCM sorption process. In this way, novel structures have been formed or stabilized as a result of such structural changes. In some cases, even forming novel phases which can be more advantageous for the storage process, e.g., inhibition of the formation of amorphous phase in magnesium sulfate composites. Overall, this phenomenon has the potential to benefit the stabilization of the thermochemical materials and should be further studied and exploited in future studies.

Supporting Information

Supporting Information is available from the Wiley Online Library or from the author.

Conflict of Interest

The authors declare no conflict of interest.

Data Availability Statement

The data that support the findings of this study are available from the corresponding author upon reasonable request.

Keywords

hybrids, manufacturing, matrix, PCM, TCM

Received: May 10, 2022
Revised: February 14, 2023
Published online: May 13, 2023

[1] P. A. J. Donkers, L. C. Sögütoglu, H. P. Huinink, H. R. Fischer, O. C. G Adan, *Appl. Energy* **2017**, *199*, 45.
[2] C. Jarrett, W. Chueh, C. Yuan, Y. Kawajiri, K. H. Sandhage, A. Henry, *Sol. Energy* **2016**, *123*, 57.
[3] A. Palacios, M. E. Navarro, C. Barreneche, Y. Ding, *Appl. Energy* **2020**, *274*, 115024.
[4] M. E. Navarro, Jiang, P. Anabel Zhu, in *Thermal Energy Storage: Materials, Devices, Systems and Applications*, Energy and Environment Series, Vol. I (Ed: Y. Ding), **2020**.
[5] L. Shere, S. Trivedi, S. Roberts, A. Sciacovelli, Y. Ding, *Heat Transfer Eng.* **2018**, *40*, 1176.
[6] L. Scapino, H. A. Zondag, J. Van Bael, J. Diriken, C. C. M Rindt, *Appl. Energy* **2017**, *190*, 920.
[7] J. N Chiu, *Inorg. Mater.* **2009**, *15*, 24.
[8] N. Yu, R. Z. Wang, L. W Wang, *Prog. Energy Combust. Sci.* **2013**, *39*, 489.
[9] Directorate-General for Energy, *Mapping and analyses of the current and future (2020–2030) heating/cooling fuel deployment (fossil/renewables)*, Energy, **2016**.
[10] B. Michel, N. Mazet, P. Neveu, *Appl. Energy* **2014**, *129*, 177.
[11] F. Marias, P. Neveu, G. Tanguy, P. Papillon, *Energy* **2014**, *66*, 757.
[12] V. M. van Essen, J. Cot Gores, L. P. J. Bleijendaal, H. A. Zondag, R. Schuitema, M. Bakker, W. G. J. Van Helden, in *ASME 2009 3rd Int. Conf. Energy Sustainability*, American society of mechanical engineers, San Francisco, Vol. 2, **2009**, pp. 825–830.
[13] G. T. Whiting, D. Grondin, D. Stosic, S. Bennici, A. Auroux, *Sol. Energy Mater. Sol. Cells* **2014**, *128*, 289.
[14] V. M. van Essen, H. A. Zondag, J. C. Gores, L. P. J. Bleijendaal, M. Bakker, R. Schuitema, W. G. J. Van Helden, C. C. M. Rindt, Z. He, *J. Sol. Energy Eng.* **2009**, *131*, 041014.
[15] S. Hongois, F. Kuznik, P. Stevens, J. J Roux, *Sol. Energy Mater. Sol. Cells* **2011**, *95*, 1831.
[16] A. Abedin, M. Rosen, J. C. Choi, S. D. Kim, T. U. Eindhoven, *Open Renewable Energy J.* **2011**, *4*, 42.
[17] L. Okhrimenko, L. Favergeon, K. Johannes, F. Kuznik, M. Pijolat, *Thermochim. Acta* **2017**, *656*, 135.
[18] H. Jarimi, D. Aydin, Z. Yanan, G. Ozankaya, X. Chen, S. Riffat, *Int. J. Low-Carbon Technol.* **2019**, *14*, 44.
[19] Y. Konuklu, F. Erzin, H. B. Akar, A. M. Turan, *Sol. Energy Mater. Sol. Cells* **2019**, *193*, 85.
[20] T. Feczkó, A. F. Kardos, L. Trif, J. Gyenis, *WIT Trans. Built Environ.* **2014**, *142*, 279.
[21] A. Asghar, Y. Abdul, R. Hashaikeh, *J. Appl. Polym. Sci.* **2012**, *125*, 2121.
[22] Y. Li, M. Wu, R. Liu, Y. Huang, *Sol. Energy Mater. Sol. Cells* **2009**, *93*, 1321.
[23] A. Fallahi, G. Guldentops, M. Tao, S. Granados-Focil, S. Van Dessel, *Appl. Therm. Eng.* **2017**, *127*, 1427.
[24] M. Roelands, R. Cuypers, K. D. Kruit, H. Oversloot, A. J. De Jong, W. Duvalois, L. Van vlief, C. Hoegaerts, *Energy Proc.* **2015**, *70*, 257.
[25] G. Drake, L. Freiberg, N. AuYeung, *Energy Technol.* **2018**, *6*, 351.
[26] H. M. Weingrill, K. Resch-Fauster, C. Zauner, *Macromol. Mater. Eng.* **2018**, *303*, 1.
[27] W. Gao, W. Lin, T. Liu, C. Xia, *Int. J. Green Energy* **2007**, *4*, 301.
[28] J. K. Fink, *Reactive Polymers Fundamentals and Applications: A Concise Guide to Industrial Polymers*, 2nd ed., William Andrew Publishing, Oxford **2013**.
[29] W. D. Li, E. Y. Ding, *Sol. Energy Mater. Sol. Cells* **2007**, *91*, 764.
[30] Z. Liu, X. Fu, L. Jiang, B. Wu, J. Wang, J. Lei, *Sol. Energy Mater. Sol. Cells* **2016**, *147*, 177.
[31] K. Peng, C. Chen, W. Pan, W. Liu, Z. Wang, L. Zhu, *Sol. Energy Mater. Sol. Cells* **2016**, *145*, 238.
[32] J. C. Su, P. S. Liu, *Energy Convers. Manage.* **2006**, *47*, 3185.
[33] C. Chen, W. Liu, Z. Wang, K. Peng, W. Pan, Q. Xie, *Sol. Energy Mater. Sol. Cells* **2015**, *134*, 80.
[34] H. M. Weingrill, K. Resch-Fauster, T. Lucyshyn, C. Zauner, *Polym. Test.* **2019**, *76*, 433.
[35] C. Zauner, F. Hengstberger, M. Etzel, D. Lager, R. Hofmann, H. Walter, *IOP Conf. Ser.: Mater. Sci. Eng.* **2017**, *251*, 012123.
[36] I. O. Salyer, J. E. Davison, *J. Appl. Polym. Sci.* **1983**, *28*, 2903.
[37] C. Yang, M. E. Navarro, B. Zhao, G. Leng, G. Xu, L. Wang, Y. Jin, Y. Ding, *Sol. Energy Mater. Sol. Cells* **2016**, *152*, 103.
[38] *Center for the Polyurethanes Industry. Working with MDI and Polymeric MDI*, **2012**.
[39] X. Li, Y. Lu, H. Wang, E. Pöselt, B. Eling, Y. Men, *Eur. Polym. J.* **2017**, *97*, 423.
[40] Y. T. Shieh, H. T. Chen, K. H. Liu, Y. K Twu, *J. Polym. Sci., Part A: Polym. Chem.* **1999**, *37*, 4126.
[41] Z. Shi, H. Xu, Q. Yang, C. Xiong, M. Zhao, K. Kobayashi, T. Saito, A. Isogai, *Carbohydr. Polym.* **2019**, *225*, 115215.
[42] C. Lu, S. W. Chiang, H. Du, J. Li, L. Gan, X. Zhang, et al., *Polymer* **2017**, *115*, 52.
[43] F. Barroso-Bujans, F. Fernandez-Alonso, S. Cerveny, S. F. Parker, A. Alegría, J. Colmenero, *Soft Matter* **2011**, *7*, 7173.

[44] C. Yang, M. E. Navarro, B. Zhao, G. Leng, G. Xu, L. Wang, Y. Jin, Y. Ding, *Sol. Energy Mater. Sol. Cells* **2016**, *152*, 103.
[45] K. Sewda, S. N Malti, *J. Appl. Polym. Sci.* **2010**, *116*, 2658.
[46] K. A. Thakare, H. G. Vishwakarma, A. G. Bhave, *Int. J. Res. Eng. Technol.* **2015**, *4*, 92.
[47] J. Gu, H. Xu, C. Wu, *Adv. Polym. Technol.* **2014**, *33*, 1.
[48] I. Tavman, Y. Aydogdu, M. Kök, A. Turgut, A. Ezan, *Arch. Mater. Sci. Eng.* **2011**, *50*, 56.
[49] L. Zhao, Z. Guo, Z. Cao, T. Zhang, Z. Fang, M. Peng, *Polym. Degrad. Stab.* **2013**, *98*, 1953.
[50] D. Shen, R. Xiao, S. Gu, H. Zhang, *IntechOpen*, **2013**, https://doi.org/10.5772/51883.
[51] A. Mihranyan, A. P. Llagostera, R. Karmhag, M. Strømme, R. Ek, *Int. J. Pharm.* **2004**, *269*, 433.
[52] K. Korhammer, M. M. Druske, A. Fopah-Lele, H. U. Rammelberg, N. Wegscheider, O. Opel, T. Osterand, W. Ruck, *Appl. Energy* **2016**, *162*, 1462.
[53] K. Korhammer, C. Apel, T. Osterland, W. K. L. Ruck, *Energy Proc.* **2016**, *91*, 161.
[54] P. A. J. Donkers, S. Beckert, L. Pel, F. Stallmach, M. Steiger, O. C. G. Adan, *J. Phys. Chem. C* **2015**, *119*, 28711.
[55] A. Fopah-Lele, J. G. Tamba, *Sol. Energy Mater. Sol. Cells* **2017**, *164*, 175.
[56] C. J. Ferchaud, H. A. Zondag, J. B. J. Veldhuis, R. De Boer, *J. Phys. Conf. Ser.* **2012**, *395*, 012069.
[57] K. D. Grevel, J. Majzlan, A. Benisek, E. Dachs, M. Steiger, A. D. Fortes, B. Marler, *Astrobiology* **2012**, *12*, 1042.
[58] M. C. Morris, H. F. McMurdie, E. H. Evans, B. Paretzkin, H. S. Parker, N. P. Pyrros, C. R. Hubbart, *Standard X-Ray Diffraction Powder Patterns*, NBS Monograph, USA **1982**.
[59] P. Xi, X. Gu, B. Cheng, Y. Wang, *Energy Convers. Manage.* **2009**, *50*, 1522.
[60] E. Ruiz-Agudo, J. D. Martín-Ramos, C. Rodriguez-Navarro, *J. Phys. Chem. B* **2007**, *111*, 41.
[61] M. Steiger, K. Linnow, H. Juling, G. Gülker, J. A. El, S. Brüggerhoff, D. Kirchnerl, *Cryst. Growth Des.* **2008**, *8*, 336.
[62] K. D. Grevel, J. Majzlan, *Geochim. Cosmochim. Acta* **2009**, *73*, 6805.
[63] P. M. Grindrod, M. J. Heap, A. D. Fortes, P. G. Meredith, I. G. Wood, F. Trippetta, P. R. Sammond, *J. Geophys. Res.* **2010**, *115*, 394.
[64] U. W. Gedde, H. S. Hedenqvist, *Morphology of semicrystalline polymers, Fundamental polymer science, Graduate texts in Physics*, **2019**, 251–326.
[65] Z. Liu, Y. Bando, J. Drennan, A. E. C. Spargo, *J. Appl. Crystallogr.* **2003**, *36*, 1026.
[66] C. Zhang, L. Li, X. Yang, J. Shi, L. Gui, J. Liu, *Int. J. Heat Mass Transfer* **2020**, *148*, 119055.
[67] A. Wang, J. J. Freeman, B. L. Jolliff, I. M. Chou, *Geochim. Cosmochim. Acta* **2006**, *70*, 6118.
[68] M. Ibrahim, H. He, *Classification of polyethylene by Raman spectroscopy*, Application Note AN52301, Thermo Fisher Scientific, **2017**, Vol. *792*.
[69] V. K. Malinovsky, A. P. Sokolov, *Solid State Commun.* **1986**, *57*, 757.
[70] M. F. Ando, O. Benzine, Z. Pan, J. L. Garden, K. Wondraczek, S. Grimm, K. Schuster, L. Wondraczek, *Sci. Rep.* **2018**, *8*, 5394.
[71] K. M. Seven, J. M. Cogen, J. F. Gilchrist, *Polym. Eng. Sci.* **2016**, *56*, 541.